Stepwise Construction of Discrete Heterometallic Coordination Cages Based on Self-Sorting Strategy

Hao Li, Ying-Feng Han, Yue-Jian Lin, Zi-Wei Guo, and Guo-Xin Jin*

Shanghai Key Laboratory of Molecular Catalysis and Innovative Material, Department of Chemistry, Fudan University, 200433, Shanghai, P. R. China

S *Supporting Information*

ABSTRACT: A chelation-directed self-sorting synthesis of a series of cationic heterometallic coordination cages (HCCs) with tunable sizes is described. Two complexation modes were found in the cage-forming process. Metal-anchoring host–guest behavior and size-selective in-cage catalytic activities were found for the HCCs.

Coordination-driven self-assembly is a promising tool for application-oriented structural manipulation of coordination macrocycles/cages.[1-3] One intriguing task in this research area is to functionalize the architectures with secondary metal sites. Synthesizing heterometallic coordination cages (HCCs) would be attractive due to the combination of open metal sites and the inner cavity (Figure 1), which can result in novel
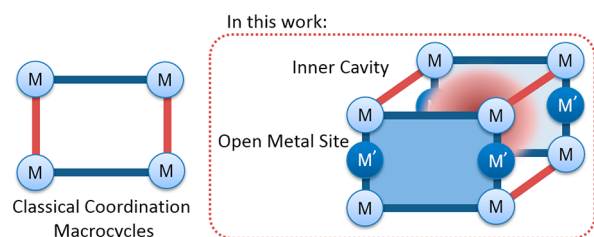

Figure 1. Representation of classical coordination macrocycles (left) and heterometallic coordination cages (right).

functionalities such as metal-anchored encapsulation and enzyme-mimicking supramolecular catalysis. In particular, there are extraordinary similarities between catalysis inside HCCs and enzyme catalysis: a combination of (i) catalytic pockets which regulate and select substrates and (ii) active sites which complete the catalysis.[4] Additionally, the homogeneous nature of HCCs, which distinguish them from the spatially infinite heterometallic metal–organic frameworks (HMOFs),[5] can mimic the individual host–guest recognition of enzymes and allows more detailed mechanistic investigations. Interesting selectivities were observed based on the size and the orientation of substrates in HCC catalysis, as is also observed in enzyme catalysis.[6]

As a candidate for use as an artificial enzyme, it is crucial that the size and the active sites of an HCC are variable to adapt different reactions and substrates. Unfortunately, the formation of HCCs is challenging due to the difficulty in achieving selective coordination, as well as their poorer structural stabilities compared with HMOFs. As a result, a universal

methodology to develop an HCC family with variable sizes and active sites is yet to be reported.[7] Recently, we have reported a series of size-extending heterometallic metallarectangles,[8] using the heteroligand synthetic strategy based on Cp*M (M = Ir, Rh) metal corners.[9] However, borromean-type ring structures that block the inner cavities were found when using long bridging ligands.[10] In this work, we introduce three-dimensional cage structures to prevent the formation of interlocking structures or interpenetration. A series of cuboid Ir–Cu, Ir–Ni, and Ir–Zn heterometallic coordination cages ([**HCC-1**]$^{8+}$–[**HCC-6**]$^{8+}$) is reported, isolated as the triflate salts, with the distances between two nearby secondary metal centers in the HCC easily controlled by adjusting the lengths of the bridging ligands. No interlocking structures or interpenetration is found in the large metal–metal separation. Metal-anchoring host–guest behavior was found inside the HCCs. A proof-of-concept catalytic investigation based on an acetalization reaction is also conducted herein, which demonstrates in-cage size selectivities using the HCC catalyst.

N,N′-1,4-Phenylenebis(oxamate) (H$_2$ppba) was chosen to build HCCs based on two considerations: (i) it can function as a bridging ligand with a pair of O^O chelating sites and a pair of O^N chelating sites and may lead to selective coordination with different metal centers; (ii) coordination of ppba to copper was reported to give a planar four-coordinate copper center,[11a] which is coordinatively unsaturated and may function as a catalytically active site. Similar coordination modes were also reported between the oxamate group and nickel/zinc.[11b]

The first step to construct HCCs is to synthesize the planar heterometallic building blocks (Scheme 1). The planar

Scheme 1. Self-Sorting Formation of Heterometallic Building Blocks
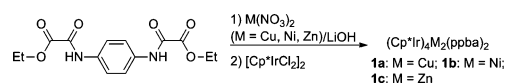
heterometallic complex **1a** was isolated as the product of a self-sorting reaction. [Cp*IrCl$_2$]$_2$ (1 equiv) was treated with the complex of Cu(NO$_3$)$_2$ and *N,N*′-1,4-phenylene-bis(oxamic acid ethyl ester) (H$_2$Et$_2$ppba) for 6 h in a solvent mixture of CH$_2$Cl$_2$/MeOH/H$_2$O. As a result of the self-sorting reaction, **1a** was isolated as a yellow precipitate. Complex **1a** has poor solubility in water, methanol, and most common organic

solvents, but is slightly soluble in acetonitrile. ESI-MS indicates a composition corresponding to $(Cp*Ir)_4Cu_2(ppba)_2Cl_4$ (Figure 2a).

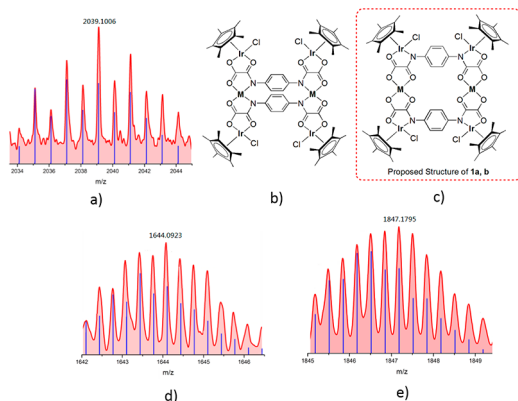**Figure 2.** (a) ESI-MS spectra of $[1a − Cl]^+$ (red: experimental, blue: theoretical); (b and c) two plausible structures of **1a**−**c**; (d) ESI-MS spectra of $[HCC-1][OTf^−]_5^{3+}$; (e) ESI-MS spectra of $[HCC-4][OTf^−]_5^{3+}$.

Complexes **1b** and **1c** were also synthesized in a similar procedure using $M(NO_3)_2$ (M = Ni, Zn) as the source of the secondary metal. The solubilities of **1b** and **1c** are even poorer than **1a**. Therefore, they cannot be characterized by ESI-MS. However, the EA analysis of the complex supports the formulation of $(Cp*Ir)_4M_2(ppba)_2Cl_4$ (M = Ni, Zn).

No structural insight into **1a**−**c** could be obtained due to their poor solubilities, preventing growth of single crystals suitable for X-ray diffraction analysis. Therefore, the exact coordination mode of **1a**−**c** cannot be determined. Although the Cu(II) centers in homometallic $[Cu_2(ppba)_2]^{4−}$ bind the O^N sites,[11a] an alternative coordination mode was proposed for heterometallic complex **1a**: copper should coordinate to the O^O site, while the iridium coordinates to the O^N site (Figure 2c). The reasons are as follows: (i) due to the electronic effects of the ancillary ligand, Cp*Ir(III) could be seen as a soft Lewis acid, whereas Cu(II) is a borderline Lewis acid.[12] Consequently, compared with copper, Cp*Ir should have more affinity to nitrogen atoms. (ii) More importantly, the structures of the HCC products of the following reaction, in which copper ions also bind the O^O sites and iridium the O^N sites, support the assumption about the structure of **1a**, as will be mentioned below. We also propose a similar structure for **1b** and **1c** for the same reasons.

Using **1a** as the building block, $[HCC-1]^{8+}$−$[HCC-4]^{8+}$ were constructed in the second assembly step. Complex **1a** was treated with AgOTf to break the Ir−Cl bonds, followed by addition of bridging ligands **L** [**L** = pyrazine, 4,4′-bipyridine (bpy), 1,2-bis(pyridin-4-yl)ethane (bpe), 1,4-bis(pyridine-4-yl)benzene (bpb)), Scheme 2]. Excess AgOTf was eliminated by adding I$^−$ anions to the solution. The formation of $[HCC-1][OTf]_8$−$[HCC-4][OTf]_8$ was characterized by ESI-MS, which indicates the complexation of two $(Cp*Ir)_4Cu_2(ppba)_2^{4+}$ moieties and four **L** molecules, along with eight OTf$^−$ counteranions. It is noteworthy that, for all cases of HCCs, no dimeric or trimeric product was detected in the ESI-MS spectra. For example, in our previous study, the bpb-linked heterometallic metallarectangle shows a trimeric structure in both ESI-MS and single-crystal X-ray studies. In contrast, in the case of HCCs, bpb-linked $[HCC-4][OTf]_8$ shows only a

Scheme 2. Stepwise Assembly of $[HCC-1]^{8+}$−$[HCC-6]^{8+}$
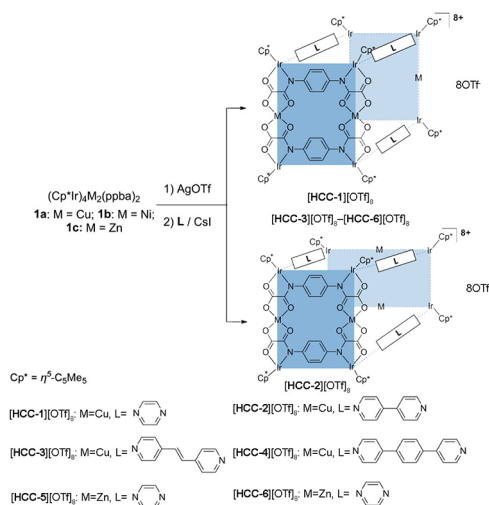
monomeric m/z peak (Figure 2e), as does the pyrazine-linked $[HCC-1][OTf]_8$ (Figure 2d). The introduction of the 3d cage structure resulted in preventing the inner cavities of HCCs from forming borromean packing and other interlocking structures. The counteranion plays an important role in the solubility of HCCs. Changing of the OTf$^−$ counterion to PF$_6^−$ or NO$_3^−$ anions will result in insoluble solids.

The structures of $[HCC-1]^{8+}$ and $[HCC-2]^{8+}$ were confirmed by single-crystal X-ray diffraction analysis of the triflate salts. Two complexation modes were found (Figure 3). The structure of $[HCC-1]^{8+}$ was found to be a cuboid-shaped cage with eight Cp*Ir units at the corners of the cuboid and two pairs of planar tetracoordinate Cu(II) units facing each other (Figure 3a,c). Each copper atom coordinates to two O^O chelating sites of two ppba units, whereas the iridium atoms coordinate to the O^N chelating sites. This structure supports

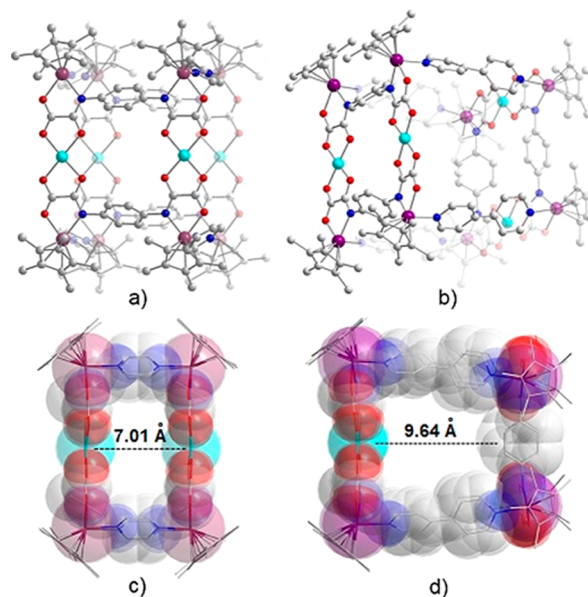**Figure 3.** (a) Molecular structure of $[HCC-1]^{8+}$; (b) molecular structure of $[HCC-2]^{8+}$; (c) side view of $[HCC-1]^{8+}$; (d) side view of $[HCC-2]^{8+}$. Purple, turquoise, blue, red, and gray represent iridium, copper, nitrogen, oxygen, and carbon atoms, respectively. Hydrogen atoms, anions, and solvent molecules have been omitted for clarity.

2983

dx.doi.org/10.1021/ja412667t | J. Am. Chem. Soc. 2014, 136, 2982−2985

our hypothesis about the structure of **1**, which has the same coordination mode. The size of the cage is $8.33 \times 10.82 \times 7.01$ Å^3 (Ir−Ir distance), with a distance of 7.01 Å between two face-to-face copper centers (Figure 3c). This distance is typical in pyrazine-bridged macrocycles/cages.[13]

Unlike [**HCC-1**]$^{8+}$, [**HCC-2**]$^{8+}$ has a distorted cage structure. The coordination mode of the (Cp*Ir)$_4$Cu$_2$(ppba)$_2$$^{4+}$ moieties in [**HCC-1**]$^{8+}$ is the same as that in [**HCC-2**]$^{8+}$, but two (Cp*Ir)$_4$Cu$_2$(ppba)$_2$$^{4+}$ fragments are distorted by 90° (Figure 3b,d). Two factors could be taken into consideration in explaining why such a distortion occurs: (i) Due to the noncoplanar nature of the two pyridine rings in bpy (the angle between two pyridine rings is 37.6°), the distorted geometry would be more thermodynamically favorable, so that the Cp* and pyridine rings could be far away from each other;[14] (ii) bpy is longer and more flexible than pyrazine; therefore it could slightly bend to cover the length difference of two distorted (Cp*Ir)$_4$Cu$_2$(ppba)$_2$$^{4+}$ moieties (8.33 Å in one direction and 10.82 Å in another). Because of the distortion, there were no face-to-face copper centers in the cage. Each copper center is facing the closest C−C bond of the opposite ppba, with a distance of 9.64 Å (Figure 3d).

Unfortunately, for [**HCC-3**][OTf]$_8$ and [**HCC-4**][OTf]$_8$, no suitable single crystal could be obtained. We propose for these a similar complexation mode to that of [**HCC-1**]$^{8+}$, in which coppers of two (Cp*Ir)$_4$Cu$_2$(ppba)$_2$$^{4+}$ face each other (Scheme 2). The proposition is based on the observation that the degree of noncoplanarity of the two pyridine groups in bpe and bpb in our previous results is much less than that in [**HCC-2**]$^{8+}$.[8]

The self-sorting strategy for the synthesis of HCCs is proven to be suitable not only for copper as the secondary metal but also for other transition metals. [**HCC-5**]$^{8+}$ and [**HCC-6**]$^{8+}$, with nickel and zinc at the second site, respectively, can be formed following the protocol similar to that of [**HCC-1**]$^{8+}$−[**HCC-4**]$^{8+}$, using **1b** and **1c** as the building blocks, and was characterized by ESI-MS.

Weak solvent interactions on the unsaturated copper sites were observed in both [**HCC-1**]$^{8+}$ and [**HCC-2**]$^{8+}$, showing that the second metal sites are "active". Each copper center in [**HCC-1**]$^{8+}$ coordinates to water molecules and methanol molecules at the direction perpendicular to the tetracoordinate plane. In [**HCC-2**]$^{8+}$, each copper atom coordinates to one OTf$^−$ anion perpendicular to the square plane outside the cage and one water molecule inside the cage. In both cases, the distances between the copper and solvent/anion oxygen atoms (2.30−2.39 Å) are significantly longer than those between the copper and oxygen atoms of ppba (1.96−1.99 Å), which indicates a much weaker coordination. Accordingly, these two water molecules could leave the copper centers easily in the catalysis process, leaving the metal centers open for substrate binding.

The "activeness" of the second metal sites could be further demonstrated by evidence of the interesting metal-anchoring host−guest behavior of HCCs. When adding excess AgOTf to the solution of [**HCC-1**]$^{8+}$, the encapsulation of AgOTf is revealed by the solid-state structure of {AgOTf ⊂ [**HCC-1**]$^{8+}$} (Figure 4a,b), in which the Ag$^+$ cations and OTf$^−$ anions are encapsulated by different interaction modes: two silver cations are trapped by the *pseudo* crown ether structures of the Cu$_2$ppba$_2$ moietes (Figure 4a), whereas two OTf$^−$ anions are found inside the cage cavities between two copper atoms (Figure 4b). This encapsulation of both anions and cations is caused by weak interactions. The distances between the copper
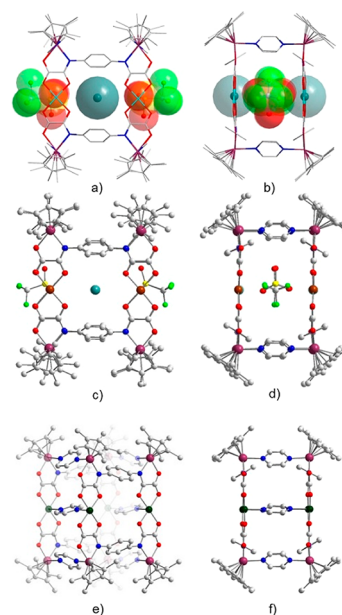

Figure 4. (a) Molecular structure of {AgOTf ⊂ [**HCC-1**]$^{8+}$}; (b) side view of {AgOTf ⊂ [**HCC-1**]$^{8+}$}; (c) cation structure of {AgOTf ⊂ [**HCC-6**]$^{8+}$}; (d) side view of {AgOTf ⊂ [**HCC-6**]$^{8+}$}; (e) cation structure of {pyrazine ⊂ [**HCC-5**]$^{8+}$}; (f) side view of {pyrazine ⊂ [**HCC-5**]$^{8+}$}. Blue gray, silver; yellow, sulfur; green, fluorine; dark green, nickel.

ions and oxygen atoms in OTf$^−$ anions are around 2.4 Å, and the distances between silver cations and oxygen atoms in ppba ligands are around 3.1−3.2 Å. Similar encapsulation behavior of AgOTf was also found in [**HCC-6**]$^{8+}$. The structure of [**HCC-6**]$^{8+}$ is similar to that of [**HCC-1**]$^{8+}$, as well as the binding mode of silver cations and OTf$^−$ anions (Figure 4c,d). Metal-anchoring encapsulation behavior was also found in [**HCC-5**]$^{8+}$. Although the crystal structure of naked [**HCC-5**]$^{8+}$ could not be obtained, when excess pyrazine was added, a pyrazine-coordinated [**HCC-5**]$^{8+}$ complex could be crystallized (Figure 4e,f).

The copper center of HCCs can be seen as a Lewis acid. Due to their heterometallic structure, the Lewis acidity of the copper centers would increase due to the strong electron withdrawing effect of the Cp*Ir group through conjugate bonds.[15] This phenomenon could benefit Lewis acid assisted catalysis using this framework. [**HCC-1**][OTf]$_8$ shows excellent size selectivity in catalyzing the acetalization of aldehydes (Table 1). Large substrates tend to be blocked by the cage and therefore cannot undergo the catalysis. Kinetic studies of [**HCC-1**][OTf]$_8$ systems support our proposition of in-cage two-center catalytic acetalization in [**HCC-1**][OTf]$_8$. In addition, [**HCC-5**][OTf]$_8$ was found to be catalytically inactive, indicating that copper is the active site in the catalytic process. These results demonstrate that the size selectivities shown in Table 1 are indeed caused by the "second-site" in-cage catalysis.[16]

In conclusion, we have developed a chelation-directed self-sorting strategy to efficiently construct a series of heterometallic metal−organic cages. The strategy can be applied to different transition metals as the second site, such as copper, nickel, and zinc. Interesting metal-anchoring host−guest behavior was observed inside the HCCs. An in-cage size-selective catalytic procedure was found for [**HCC-1**][OTf]$_8$. We believe that our synthetic strategy can allow us to develop a larger HCC family with increased structural complexity and controllability to

Table 1. Competitive Acetalizations with [HCC-1][OTf]$_8$[a]

entry	substrate	additive[b]	yield [%][c]
1	benzaldehyde + 2a	–	3: 80
			4a: 13
2	benzaldehyde + 2a	benzonitrile	3: 94
			4a: trace
3	benzaldehyde + 2b	benzonitrile	3: 92
			4b: 11
4	benzaldehyde + 2c	benzonitrile	3: 89
			4c: 24

[a]Reaction conditions: aldehyde (0.5 mmol), catalyst (0.005 mmol) in CH$_3$NO$_2$/MeOH (2:3). [b]0.5 mmol. [c]Determined by GC analysis using naphthalene or methylbenzene as internal standard.

provide better candidates for enzyme-mimicking (biomimetic) catalysis. We are currently trying to control the cage-refined environment of the active sites by ligand modification.

■ ASSOCIATED CONTENT

Ⓢ Supporting Information

Experimental procedures, characterization data, catalytic study, mechanistic study, kinetic investigation and crystallographic data for [HCC-1][OTf]$_8$, [HCC-2][OTf]$_8$, {AgOTf ⊂ [HCC-1][OTf]$_8$}, {AgOTf ⊂ [HCC-6][OTf]$_8$}, and {pyrazine ⊂ [HCC-5][OTf]$_8$} (in CIF format). This material is available free of charge via the Internet at http://pubs.acs.org.

■ AUTHOR INFORMATION

Corresponding Author

gxjin@fudan.edu.cn

Notes

The authors declare no competing financial interest.

■ ACKNOWLEDGMENTS

■ REFERENCES

(1) For reviews of coordination-driven self-assembly, see: (a) Cook, T. R.; Zheng, Y. R.; Stang, P. J. *Chem. Rev.* **2013**, *113*, 734. (b) Cook, T. R.; Vajpayee, V.; Lee, M. H.; Stang, P. J.; Chi, K.-W. *Acc. Chem. Res.* **2013**, *46*, 2464. (c) Chakrabarty, R.; Mukherjee, P. S.; Stang, P. J. *Chem. Rev.* **2011**, *111*, 6810. (d) Northrop, B. H.; Zheng, Y. R.; Chi, K. W.; Stang, P. J. *Acc. Chem. Res.* **2009**, *42*, 1554. (e) Northrop, B. H.; Yang, H.-B.; Stang, P. J. *Chem. Commun.* **2008**, 5896. (f) Gianneschi, N. C.; Masar, M. S., III; Mirkin, C. A. *Acc. Chem. Res.* **2005**, *38*, 825. (g) Leininger, S.; Olenyuk, B.; Stang, P. J. *Chem. Rev.* **2000**, *100*, 853. (h) Stang, P. J.; Olenyuk, B. *Acc. Chem. Res.* **1997**, *30*, 502.

(2) For reviews of application-oriented structure manipulation, see: (a) Li, S.; Huang, J.; Cook, T. R.; Pollock, J. B.; Kim, H.; Chi, K.-W.; Stang, P. J. *J. Am. Chem. Soc.* **2013**, *135*, 2084. (b) Han, Y.-F.; Li, H.; Jin, G.-X. *Chem. Commun.* **2010**, *46*, 6879. (c) Yoshizawa, M.; Klosterman, J. K.; Fujita, M. *Angew. Chem., Int. Ed.* **2009**, *48*, 3418.

(d) Therrien, B. *Eur. J. Inorg. Chem.* **2009**, 2445. (e) Severin, K. *Chem. Commun.* **2006**, 3859.

(3) Selected examples include: (a) Han, Y.-F.; Jin, G.-X.; Hahn, F. E. *J. Am. Chem. Soc.* **2013**, *135*, 9263. (b) Riddell, I. A.; Smulders, M. M. J.; Clegg, J. K.; Hristova, Y. R.; Breiner, B.; Thoburn, J. D.; Nitschke, J. R. *Nat. Chem.* **2012**, *4*, 751. (c) Conrady, F. M.; Fröhlich, R.; Brinke, C. S.; Pape, T.; Hahn, F. E. *J. Am. Chem. Soc.* **2011**, *133*, 11496. (d) Han, Y.-F.; Jia, W.-G.; Lin, Y.-J.; Jin, G.-X. *Angew. Chem., Int. Ed.* **2009**, *48*, 6234. (e) Therrien, B.; Süss-Fink, G.; Govindaswamy, P.; Renfrew, A. K.; Dyson, P. J. *Angew. Chem., Int. Ed.* **2008**, *47*, 3773. (f) Shan, N.; Vickers, S. J.; Adams, H.; Ward, M. D.; Thomas, J. A. *Angew. Chem., Int. Ed.* **2004**, *43*, 3938. (g) Lehaire, M.-L.; Scopelliti, R.; Piotrowski, H.; Severin, K. *Angew. Chem., Int. Ed.* **2002**, *41*, 1419.

(4) Wiester, M. J.; Ulmann, P. A.; Mirkin, C. A. *Angew. Chem., Int. Ed.* **2011**, *50*, 114.

(5) (a) Zhu, C.; Yuan, G.; Chen, X.; Yang, Z.; Cui, Y. *J. Am. Chem. Soc.* **2012**, *134*, 8058. (b) Farha, O. K.; Shultz, A. M.; Sarjeant, A. A.; Nguyen, S. T.; Hupp, J. T. *J. Am. Chem. Soc.* **2011**, *133*, 5652. (c) Das, M. C.; Xiang, S.; Zhang, Z.; Chen, B. *Angew. Chem., Int. Ed.* **2011**, *50*, 10510. (d) Halper, S. R.; Do, L.; Stork, J. R.; Cohen, S. R. *J. Am. Chem. Soc.* **2006**, *128*, 15255.

(6) (a) Lee, S. J.; Cho, S.-H.; Mulfort, K. L.; Tiede, D. M.; Hupp, J. T.; Nguyen, S. T. *J. Am. Chem. Soc.* **2008**, *130*, 16828. (b) Masar, M. S., III; Gianneschi, N. C.; Oliveri, C. G.; Stern, C. L.; Nguyen, S. T.; Mirkin, C. A. *J. Am. Chem. Soc.* **2007**, *129*, 10149.

(7) Examples include: (a) Smulders, M. M.; Jiménez, A.; Nitschke, J. R. *Angew. Chem., Int. Ed.* **2012**, *51*, 6681. (b) Wu, H.-B.; Wang, Q.-M. *Angew. Chem., Int. Ed.* **2009**, *48*, 7343. (c) de Wolf, P.; Waywell, P.; Hanson, M.; Heath, S. L.; Meijer, A. J. H. M.; Teat, S. J.; Thomas, J. A. *Chem.—Eur. J.* **2006**, *12*, 2188. (d) Sun, S.-S.; Stern, C. L.; Nguyen, S. T.; Hupp, J. T. *J. Am. Chem. Soc.* **2004**, *126*, 6314. (e) Sun, X.; Johnson, D. W.; Caulder, D. L.; Raymond, K. N.; Wong, E. H. *J. Am. Chem. Soc.* **2001**, *123*, 2752. (f) Merlau, M. L.; del Pilar Mejia, M.; Nguyen, S. T.; Hupp, J. T. *Angew. Chem., Int. Ed.* **2001**, *40*, 4239.

(8) Huang, S.-L.; Lin, Y.-J.; Hor, T. S. A.; Jin, G.-X. *J. Am. Chem. Soc.* **2013**, *135*, 8125.

(9) Han, Y.-F.; Jia, W.-G.; Yu, W.-B.; Jin, G.-X. *Chem. Soc. Rev.* **2009**, *38*, 3419 and references therein.

(10) Apart from our group's work, similar interlocking structures were also reported using long bridging ligands: Vajpayee, V.; Song, Y. H.; Cook, T. R.; Kim, H.; Lee, Y.; Stang, P. J.; Chi, K. W. *J. Am. Chem. Soc.* **2011**, *133*, 19646.

(11) (a) Pardo, E.; Faus, J.; Julve, M.; Lloret, F.; Muñoz, M. C.; Cano, J.; Ottenwaelder, X.; Journaux, Y.; Carrasco, R.; Blay, G.; Fernández, I.; Ruiz-García, R. *J. Am. Chem. Soc.* **2003**, *125*, 10770. (b) Sönmez, M.; Çelebı, M.; Leventa, A.; Berberb, İ.; Şentürka, Z. *J. Coord. Chem.* **2010**, *63*, 848.

(12) (a) Letko, C. S.; Heiden, Z. M.; Rauchfuss, T. B.; Wilson, S. R. *Inorg. Chem.* **2011**, *50*, 5558. (b) Heiden, Z. M.; Gorecki, B. J.; Rauchfuss, T. B. *Organometallics* **2008**, *27*, 1542. (c) Miessler, G. L.; Tarr, D. A. *Inorganic Chemistry*, 2nd ed.; Prentice-Hall: 1999.

(13) (a) Li, H.; Han, Y.-F.; Jin, G.-X. *Dalton Trans.* **2011**, *40*, 4982. (b) Han, Y.-F.; Lin, Y.-J.; Jia, W.-G.; Jin, G.-X. *Organometallics* **2008**, *27*, 4088.

(14) In our previous research, we have found an example of unexpected metallomacrocycles using non-coplanar bridging ligands: Wang, G.-L.; Lin, Y.-J.; Berke, H.; Jin, G.-X. *Inorg. Chem.* **2010**, *49*, 2193.

(15) A similar effect in a multi-Lewis acid complex can be seen in: Futatsugi, K.; Yamamoto, H. *Angew. Chem., Int. Ed.* **2005**, *44*, 1484.

(16) Detailed mechanistic and kinetic investigations are described in the Supporting Information.